MAXIMAL OIL RECOVERY BY SIMULTANEOUS CONDENSATION OF ALKANE AND STEAM

J. BRUINING AND D. MARCHESIN

ABSTRACT. This paper deals with the application of steam to enhance the recovery from petroleum reservoirs. We formulate a mathematical and numerical model that simulates co-injection of volatile oil with steam into a porous rock in a one dimensional setting. We utilize the mathematical theory of conservation laws to validate the numerical simulations. This combined numerical and analytical approach reveals the detailed mechanism for thermal displacement of oil mixtures discovered in laboratory experiments. We study the structure of the solution and the recovery as a function of the boiling point of the volatile oil, which is the most crucial parameter. The most striking result is that when the boiling point of the volatile oil is such that it condenses and stays at the location where the steam condenses also, the oil recovery is virtually complete.

1. INTRODUCTION

Steam drive is an economical way of producing oil and is used world wide for heavy oil. An overview of the last forty years of steam drive recovery in California is given in reference [18]. Steam drive is also considered an efficient method to clean polluted sites [3] [23], [35]. During the steam drive, however, a certain amount of oil is left behind in the steam swept zone [6].

In the late seventies Dietz [6] proposed to add small amounts of volatile oil to the steam to reduce the oil left behind. Similar ideas were put forward independently by Farouq-Ali [1]. The volatile oil co-injected with the steam in almost infinitesimal amounts would ideally condense at the same location where the steam condenses. The condensed volatile oil acts as a solvent for the heavy oil. As such it pushes the oil away from the steam swept zone leaving no oil behind (see Fig. 2.1). Experiments investigating the mechanism are described in references [1], [6], [10], [31] and [37]. However, there was a discrepancy between the original idea and the experimental observations. At least 5 weight % (volatile oil/water) was required to reduce considerably the saturation of the oil left behind [6]. However, it is possible that the requirement of this large percentage was caused by transient effects in the experiments. One of the goals of this paper is to clarify this point. Willman in his pioneering experiment in 1961 used a large percentage of initially present volatile oil [37]. His experiment led to the belief that any volatile oil component, initially present in the oil, would lead to virtually complete recovery from the steam swept zone. Therefore, the virtue of adding volatile oil was criticized at the time. The second goal of the paper is to establish the difference between steam drive recovery with co-injection of volatile oil and recovery of oil already containing

Key words and phrases. Porous medium, steamdrive, distillation, multiphase flow.

This work was supported in part by: CNPq Grant 301532/2003-6, FAPERJ under Grant E-26/152.163/2002. NSF through IMA (Univ. of Minnesota), Dietz Laboratory (TU Delft, The Netherlands), IMPA (Brazil).

a fraction of volatile oil. It can be expected that an efficient condensed volatile oil region is very short, shorter than the resolution of standard simulators.

Our approach [7], [8], [9], [11] is to simplify the model equations in such a way that the essential elements are retained [25] yet avoiding the complexities of solving pressure equations and non-linear compositional equations at every grid cell. As such the model is a straightforward extension of a 1-D model proposed by [32], but allowing for immiscible three-phase flow in the steam zone [38], [40] (see also [22]). The simplification is accomplished by the assumption that as to the thermodynamic behavior the steam drive runs at constant pressure; any accumulation of fluids that would lead to a pressure increase causes an immediate production of these fluids. Therefore without solving the pressure equation and solving the transport equations locally we can reach resolutions that cannot be attained in standard simulators.

These approximations allow us to find the time asymptotic solution analytically, using the method of characteristics. Knowing the analytical solution has three advantages. Firstly, this asymptotic solution is more relevant for the solution at the field scale. Secondly, it allows us to validate the numerical solution. Thirdly, it allows the study of bifurcation phenomena, i.e. change of structure of solutions under different injection conditions. The bifurcations of this model in the absence of thermal effects are described in [15], [17], [20], [21]. (See also the review in the appendix of [26]).

The model we used carries three important simplifications. Firstly, the diffusional mixings between volatile oil and heavy oil in the liquid phase and between volatile oil vapor and water vapor in the gaseous phase are disregarded. Secondly, we do not take into account the mixing of phases by ignoring capillary efftects. This measn that the model is not valid for extremely low injection rates. Finally, we do not specify a detailed model for the kinetics of the condensation process [11]. These aspects determine the internal structure of the shocks, which sometimes affect the structure of the whole Riemann solution, and are subjects for future work [20].

Section 2 describes the physical model and the relevant thermodynamic relations. The flow is described by balance equations in Section 3. The analysis of the self-similar waves viz. rarefaction and shocks is done in section 4. An implicit finite difference method requiring the solution of small matrices is described in Section 5. Section 6 summarizes earlier results on the injection of steam displacing heavy oil. Our results concerning the solution structure and the recovery in terms of the boiling point of volatile oil are discussed in Section 7. We summarize our conclusions in Section 8. Appendix A describes physical quantities, symbols and values.

2. Physical model

2.1. **Flow of fluids.** The model is based on conventional models for steam drive [12], [28]. We consider the injection of steam and volatile oil into a linear horizontal porous rock cylinder with constant porosity and absolute permeability (see Fig. 2.1). The tube is completely thermally isolated. The injection temperature is determined by the three-phase equilibrium condition for the given volatile oil/steam injection ratio. The cylinder is originally filled with oil and water. The oil consists of dead oil with or without volatile oil. By dead oil we mean oil with negligible vapor pressure. Three-phase flow occurs in the high temperature zone, while oil and water flow occurs in the low temperature zone. The fluids are in local thermodynamic equilibrium. Physical quantities are evaluated at a representative constant

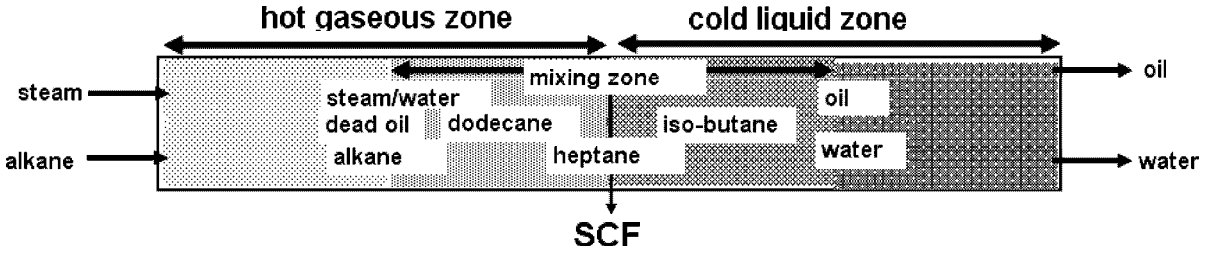

FIGURE 2.1. The porous rock cylinder. Steam and alkane are injected from the left, fluids are produced at the right. In most cases, the hot gaseous zone is sharply separated from the cold liquid zone by the steam condensation front (SCF). Initially the rock is filled with an oil mixture (oil) and water. One of three alkanes are used; dodecane has a tendency to stay upstream of the SCF, iso-butane downstream of the SCF; heptane is in between.

pressure throughout the cylinder; this is a good approximation if the total pressure variation is small relative to the total pressure. It is certainly valid in laboratory experiments. Thermal expansion of liquids is disregarded. All fluids are considered incompressible. We assume Darcy's law for multiphase flow [5], [16]. The cylinder diameter is so small that capillary forces equalize the saturation in the radial direction and temperature is homogeneous radially. As the flow is horizontal we ignore gravity effects.

2.2. **Thermodynamic fundaments.** Our interest is confined to (1) three-phase flow, i.e. flow of the aqueous (w), oleic (o) and gaseous (g) phases in the steam zone and (2) two-phase flow, i.e. flow of the aqueous and oleic phases in the liquid zone. We use the following convention: the first subscript (w, o, g) refers to the phase, the second subscript (w, v, d) refers to the component. The densities of the pure liquids, i.e., water, volatile oil and dead oil are denoted as ρ_W, ρ_V and ρ_D. The densities of the pure vapors, i.e., water and volatile oil are denoted by ρ_{gW}, ρ_{gV}.

We disregard any heat or volume contraction effects resulting from mixing. The concentration $[kg/m^3]$ of (dead) volatile oil in the oleic phase is denoted as (ρ_{od}) ρ_{ov}. The concentration of the volatile oil (water vapor) in the gaseous phase is ρ_{gv} (ρ_{gw}). For ideal fluids we obtain

$$\frac{\rho_{ov}}{\rho_V} + \frac{\rho_{od}}{\rho_D} = 1; \quad \frac{\rho_{gw}}{\rho_{gW}} + \frac{\rho_{gv}}{\rho_{gV}} = 1. \tag{2.1}$$

The densities of the pure liquids ρ_V, ρ_D $[kg/m^3]$ are considered to be independent of temperature, and the densities of the pure vapor to obey the ideal gas law, i.e.,

$$\rho_{gW} = \frac{M_W P}{RT}; \quad \rho_{gV} = \frac{M_V P}{RT}, \tag{2.2}$$

where M_W, M_V denote the molar weights of water and volatile oil respectively. T the temperature and the gas constant is $R = 8.31[J/mol/K]$. P is not a variable in this problem, but the fixed prevailing pressure value; here we use one atmosphere.

The pure water vapor pressure P_w is determined by the Clausius-Clapeyron equation [27]

$$P_w(T) = P_o \exp\left(\frac{-M_W \Lambda_W (T_b^w)}{R}\left(\frac{1}{T} - \frac{1}{T_b^w}\right)\right), \tag{2.3}$$

where $\Lambda_W\left(T_b^w\right)\left[J/kg\right]$ is its evaporation heat at its normal boiling temperature $T_b^w\left[K\right]$ at P_o, the atmospheric pressure. We also use Clausius-Clapeyron for the volatile oil vapor pressure. In addition, we use Raoult's law [27], which states that the vapor pressure of volatile oil is equal to its pure vapor pressure times the mole fraction x_{ov} of volatile oil in the oil phase. Therefore we obtain

$$P_v\left(T\right) = x_{ov} P_o \exp\left(\frac{-M_V \Lambda_V\left(T_b^v\right)}{R}\left(\frac{1}{T} - \frac{1}{T_b^v}\right)\right), \tag{2.4}$$

where $\Lambda_V\left(T_b^v\right)$ is its evaporation heat at its normal boiling temperature T_b^v. We assume that the prevailing pressure P is the sum of the two vapor pressures. From Eqs. (2.3), (2.4) and $P = P_w\left(T\right) + P_v\left(T\right)$, we find for the mole fraction in the liquid phase $x_{ov}\left(T\right)$

$$x_{ov}\left(T\right) = \frac{\frac{\rho_{ov}}{M_V}}{\frac{\rho_{ov}}{M_V} + \frac{\rho_{od}}{M_D}} = \frac{P - P_o \exp\left(\frac{-M_W \Lambda_W\left(T_b^w\right)}{R}\left(\frac{1}{T} - \frac{1}{T_b^w}\right)\right)}{P_o \exp\left(\frac{-M_V \Lambda_V\left(T_b^v\right)}{R}\left(\frac{1}{T} - \frac{1}{T_b^v}\right)\right)}. \tag{2.5}$$

From this we derive an expression for the volatile oil concentration in the oleic liquid phase

$$\rho_{ov} = \frac{x_{ov}\rho_D \rho_V M_V}{x_{ov}\rho_D M_V + \left(1 - x_{ov}\right)\rho_V M_D}. \tag{2.6}$$

Note that in the vapor no dead oil component is present, whereas in the oleic liquid phase volatile and dead oil are present. Equation (2.5) is used in Figure 6.1 left (l) (based on heptane as volatile oil component) to find the lower branch Γ extending from $\left(y_{gv}, T\right) = \left(0.0, 373.15K\right) \rightarrow \left(0.528, 352.35\right)$, where y_{gv} denotes the mole fraction of volatile oil in the vapor phase. In Figure 6.1(l) we assume that the prevailing pressure is atmospheric.

Figure 6.1(l) is a projection of the 3-D figure containing the temperature as the vertical axis, the volatile oil fraction in the vapor phase y_{gv} as the horizontal axis and the composition of the oil x_{ov} as the axis perpendicular to the paper. The projection is on a surface for which x_{ov} =constant, say the $x_{ov} = 1$ plane. As a result Figure 6.1(l) contains four phase diagrams i.e., for $x_{ov} = 1$, 0.6, 0.4, 0.2. Consider, as an example the phase diagram for $x_{ov} = 0.4$ i.e. the behavior of a dead oil/volatile oil mixture with a liquid volatile oil mole fraction of $x_{ov} = 0.4$. This phase diagram consists of the curve $x_{ov} = 0.4$ and the part of the curve Γ left of its intersection point. Below these curves the system is in the liquid phase, where oil with $x_{ov} = 0.4$ is in equilibrium with pure water. At the curve $x_{ov} = 0.4$, i.e. to the right of the intersection point of these curves, liquid oil with composition $x_{ov} = 0.4$ is in equilibrium with the vapor with a volatile oil fraction read from the horizontal axis. Left from the intersection point pure liquid water is in equilibrium with vapor with a volatile oil fraction read from the horizontal axis. At the intersection point liquid oil with composition $x_{ov} = 0.4$ is in equilibrium with liquid water and vapor with a composition read from the horizontal axis. Above these curves there is only vapor. As in all cases considered by us we have liquid water, we only use the curve Γ for the three-phase zone and below it for the two-phase zone.

We use Eq. (2.5) to compute $x_{ov}\left(T\right)$ and substitute $x_{ov}\left(T\right)$ in Eq. (2.4) to find $y_{gv}\left(T\right) = P_v\left(T\right)/P$, which is plotted on the horizontal axis. The temperature $T_{az}\left(AZ\right)$, which is 352.35 for heptane, is the lower end of this curve and corresponds to a value for which $x_{ov}\left(T_{az}\right) = 1$, the azeotropic point of the pure volatile oil-water mixture. The procedure to find the branches $\left(x_{ov} = 0.2, 0.4, 0.6, 1.0\right)$ emanating from this curve Γ is as follows. Choose

a value for x_{ov}. Apply Eq. (2.5) to obtain the plot of T versus y_{gv}. For $x_{ov} = 1$ there is only volatile oil, so the curve describes the conditions where there is water only as a vapor, volatile oil vapor, and liquid volatile oil. For $x_{ov} < 1$ there is also dead oil present but no liquid water except at the intersection point with Γ. Therefore these branches $x_{ov} = 0.2, 0.4, 0.6, 1.0$ describe the two-phase (oleic-gas) situation. For $x_{ov} = 0.2$ the system below part of the branch Γ and the branch $x_{ov} = 0.2$ is in the liquid two-phase oil/water region. The same holds for other values of x_{ov}. We can use (2.5) to obtain expressions for the concentrations $\rho_{ov}(T), \rho_{od}(T), \rho_{gw}(T)$ and $\rho_{gv}(T)$.

3. Balance equations

The energy conservation equation in terms of enthalpy is given as [4]:

$$\frac{\partial}{\partial t}\big(H_r + \varphi S_w \rho_W h_W + \varphi S_o\left(\rho_{ov} h_{oV} + \rho_{od} h_{oD}\right) + \varphi S_g\left(\rho_{gw} h_{gW} + \rho_{gv} h_{gV}\right)\big)$$
$$+ \frac{\partial}{\partial x} u\big(f_w \rho_W h_W + f_o\left(\rho_{ov} h_{oV} + \rho_{od} h_{oD}\right) + f_g\left(\rho_{gw} h_{gW} + \rho_{gv} h_{gV}\right)\big) = 0. \tag{3.1}$$

The enthalpies h are all per unit mass and depend on temperature (and on the fixed pressure). The enthalpy of steam in the gaseous phase is h_{gW}, and h_W is the enthalpy of water in the liquid aqueous phase, while h_{gV} is the enthalpy of volatile oil in the gaseous phase. Furthermore h_{oV} and h_{oD} are the enthalpies of liquid volatile oil and dead oil. The rock enthalpy H_r is per unit volume. The saturation of the oleic, aqueous and gaseous phases are S_o, S_w, S_g, while f_o, f_w, f_g are their fluxes, defined in Eq. (A.16).We use u to denote the total Darcy flow velocity and φ the constant rock porosity. We can write for the mass conservation equations of water, volatile oil, and total oil in the steam zone [24],

$$\begin{aligned}
\varphi\frac{\partial}{\partial t}\left(\rho_{gw} S_g + \rho_W S_w\right) + \frac{\partial}{\partial x} u\left(\rho_{gw} f_g + \rho_W f_w\right) &= 0,\\
\varphi\frac{\partial}{\partial t}\left(\rho_{gv} S_g + \rho_{ov} S_o\right) + \frac{\partial}{\partial x} u\left(\rho_{gv} f_g + \rho_{ov} f_o\right) &= 0,\\
\varphi\frac{\partial}{\partial t}\left(\frac{\rho_{gv}}{\rho_V} S_g + S_o\right) + \frac{\partial}{\partial x} u\left(\frac{\rho_{gv}}{\rho_V} f_g + f_o\right) &= 0.
\end{aligned} \tag{3.2}$$

Eqs. (3.2) and (3.1) can be written in condensed form as

$$\frac{\partial}{\partial t} G_\ell + \frac{\partial}{\partial x} u F_\ell = 0, \qquad \text{for} \qquad \ell = w, v, o, T. \tag{3.3}$$

We use the subscript ℓ to denote the components (w, v, o) and the energy (T). Notice that F_i are functions of the variables S_w, S_g, T. The dependent variables of Eq. (3.3) are S_w, S_g, T and u. In the two-phase zone Eqs. (3.2) and (3.1) simplify by using $\rho_{gw} = \rho_{gv} = 0$. Here f_w depends on S_w and T, f_o on S_w, $\rho_{o,v}$ and T. The dependent variables in the two-phase zone in Eq. (3.3) are S_w, $\rho_{o,v}$, T and u.

4. Analysis of elementary waves

Considering Eqs. (3.3) and the fact that we use constant injection conditions and homogeneous initial data we observe that must exist solutions that are invariant with respect to scaling $x \to ax$, $t \to at$, where a is any positive constant. Such solutions only depend on

the similarity coordinate x/t and are called Riemann solutions. These solutions represent large-time asymptotic solutions for many initial and boundary data. Standard theory of conservation laws say that Riemann solutions consist of sequences of smooth rarefaction waves, discontinuities or shocks and constant states. Shock waves satisfy the Rankine-Hugoniot (RH) conditions, which express mass conservation. We refer the interested reader to Smoller [33] and Dafermos [13]. Excellent engineering introductions in this field can be found in the papers by Pope [30], Hirasaki [19] and Dumoré, Hagoort and Risseeuw [14] and in the book by Lake [24].

We find explicit formulae for the Rankine-Hugoniot (RH) conditions, relating the wave speed with left and right states of shocks and condensation waves. We derive the characteristic speeds for rarefaction waves. We have also obtained the rarefaction curves, which represent the rarefaction waves, but we omit their lengthy derivations here. We have used these formulae to verify the correctness of every single wave found numerically in Section 7. The concatenation of the waves according to speed and the extended Lax entropy conditions [33], [13] were verified as well. As far as the authors are concerned the treatment of the velocity variable is original as there are no time derivatives for this variable in the equations.

4.1. **Shocks.** The RH conditions for (3.2) and (3.1) can be written as follows, for a shock with speed v and left and right states $(-)$ and $(+)$, in terms of the normalized quantities $\widetilde{v} := \varphi v/u^-$, $\tilde{u}^+ := u^+/u^-$:

$$
\begin{aligned}
&-\widetilde{v}\left((\rho_W S_w)^+ - (\rho_W S_w)^-\right) + (\widetilde{u}\rho_W f_w)^+ - (\rho_W f_w)^- + \\
&-\widetilde{v}\left((\rho_{gw} S_g)^+ - (\rho_{gw} S_g)^-\right) + (\widetilde{u}\rho_{gw} f_g)^+ - (\rho_{gw} f_g)^- = 0, \qquad (4.1)\\
&-\widetilde{v}\left((\rho_{ov} S_o)^+ - (\rho_{ov} S_o)^-\right) + (\widetilde{u}\rho_{ov} f_o)^+ - (\rho_{ov} f_o)^- + \\
&-\widetilde{v}\left((\rho_{gv} S_g)^+ - (\rho_{gv} S_g)^-\right) + (\widetilde{u}\rho_{gv} f_g)^+ - (\rho_{gv} f_g)^- = 0, \qquad (4.2)\\
&-\widetilde{v}\left(\left(\frac{\rho_{gv}}{\rho_V} S_g + S_o\right)^+ - \left(\frac{\rho_{gv}}{\rho_V} S_g + S_o\right)^-\right) + \left(\frac{\rho_{gv}}{\rho_V} u f_g + u f_o\right)^+ - \left(\frac{\rho_{gv}}{\rho_V} f_g + f_o\right)^- = 0, \qquad (4.3)
\end{aligned}
$$

and

$$
\begin{aligned}
&-\widetilde{v}\Big((H_r/\varphi + H_W S_w + H_o S_o + H_g S_g)^+ - (H_r/\varphi + H_W S_w + H_o S_o + H_g S_g)^-\Big)\\
&+\left(\widetilde{u}(H_W f_w + H_o f_o + H_g f_g)\right)^+ - \left(H_W f_w + H_o f_o + H_g f_g\right)^- = 0, \qquad (4.4)
\end{aligned}
$$

where the enthalpies per unit volume H_r, H_W etc. are defined in the Table in the Appendix.

We distinguish six kinds of shocks. (1) The volatile oil evaporation shock (speed v_E), with three-phase conditions at the left. Its main feature is that the volatile oil concentration increases in the downstream (right) direction. The temperature, saturations, and velocity change across the shock. (2) The steam condensation shock (speed v_{SCF}), with a three-phase condition at the left. The vapor saturation decreases drastically in the downstream direction. Again all the quantities change across the shock. (3) The volatile oil condensation shock (speed v_C), with a three-phase condition at the left. The volatile oil concentration decreases in the downstream direction. (4) The volatile oil two-phase composition shock (speed v_v), which is a contact discontinuity. A contact discontinuity represents the moving interface between two fluids in the same phase. In reality there is always diffusion, which

mixes the fluids and such an interface is an idealization. In loose mathematical terms, a contact discontinuity is defined as a shock for which the characteristic speeds to the right and to the left are equal to the shock speed. (5) The saturation shock (speed v_S). Only the saturations change, while temperature, composition and the velocity are constant, so that Eq. (4.4) does not play a role. (6) The Buckley-Leverett shock (speed v_{BL}), with only the liquid oil and water phases present. All quantities except the liquid saturations are constant, so that Eq. (4.4) again does not play a role.

4.2. **Characteristic speeds.** Using G_ℓ and F_ℓ from Eq. (3.3), we define

$$G_{\ell n} = \frac{\partial G_\ell}{\partial \mathcal{V}_n}, F_{\ell n} = \frac{\partial F_\ell}{\partial \mathcal{V}_n}, F_{\ell u} = \frac{\partial}{\partial u}\left(uF_\ell\right) = F_\ell, \tag{4.5}$$

where $(\mathcal{V}_1, \mathcal{V}_2, \mathcal{V}_3) = (S_w, S_g, T)$. Note that G_ℓ does not depend on u. Eq. (3.3) becomes:

$$\sum_{n=w,g,T}\left(G_{\ell n}\frac{\partial \mathcal{V}_n}{\partial t}\right) + \sum_{n=w,g,T}\left(uF_{\ell n}\frac{\partial \mathcal{V}_n}{\partial x}\right) + F_\ell \frac{\partial u}{\partial x} = 0, \qquad \text{for} \qquad \ell = w, v, o, T. \tag{4.6}$$

Without loss of generality $u > 0$ and the previous equations can be rewritten as

$$\sum_{n=w,g,T}\left(G_{\ell n}\frac{\partial \mathcal{V}_n}{\partial t}\right) + \sum_{n=w,g,T}\left(uF_{\ell n}\frac{\partial \mathcal{V}_n}{\partial x}\right) + F_\ell u \frac{\partial \ln u}{\partial x} = 0, \qquad \text{for} \qquad \ell = w, v, o, T. \tag{4.7}$$

Let us consider solutions of Eq. (3.3) that depend on (x, t) through the similarity coordinate $\eta = x/t$. Then Eq. (4.7) becomes

$$M^{(4)}(S_w, S_g, T, \frac{\eta}{u})\frac{d}{d\eta}(S_w, S_g, T, \ln u)^\dagger = 0, \tag{4.8}$$

where

$$M^{(4)}(\mathcal{V}, \lambda) = \begin{pmatrix} F_{11} - \lambda G_{11} & F_{12} - \lambda G_{12} & F_{13} - \lambda G_{13} & F_1 \\ F_{21} - \lambda G_{21} & F_{22} - \lambda G_{22} & F_{23} - \lambda G_{23} & F_2 \\ F_{31} - \lambda G_{31} & F_{32} - \lambda G_{32} & F_{33} - \lambda G_{33} & F_3 \\ F_{41} - \lambda G_{41} & F_{42} - \lambda G_{42} & F_{43} - \lambda G_{43} & F_4 \end{pmatrix}, \tag{4.9}$$

with $(S_w, S_g, T, \ln u)^\dagger$ denoting a column vector, $\lambda = \eta/u$, and $\mathcal{V} = (S_w, S_g, T)^\dagger$. We have replaced the subscripts w, v, o, T by $1, 2, 3, 4$.

4.2.1. *Three-phase flow.* The three characteristic speeds, i.e. the eigenvalues λ of $M^{(4)}$ can be found by a tedious calculation, which we outline here. We observe that making the determinant of (4.9) equal to zero leads to a polynomial equation of third order in λ. Indeed, after performing Gaussian elimination on the matrix (4.9), its determinant becomes the following, where A_1, A_3, A_2, A^0_{23}, A^1_{23}, $\mathcal{F}_4$, $\mathcal{F}_{43}$, and $\mathcal{G}_{43}$ depend on $\mathcal{V}$, while $A_{13}(\lambda)$, $A_{33}(\lambda)$ are linear expressions in λ with coefficients that depend on $\mathcal{V}$. Hence we find

$$\begin{vmatrix} \frac{\partial f_w}{\partial S_w} - \lambda\varphi & \frac{\partial f_w}{\partial S_g} & A_{13}(\lambda) & A_1 \\ \frac{\partial f_g}{\partial S_w} & \frac{\partial f_g}{\partial S_g} - \lambda\varphi & A_{33}(\lambda) & A_3 \\ 0 & 0 & A^0_{23} - \lambda A^1_{23} & A_2 \\ 0 & 0 & \mathcal{F}_{43} - \lambda\mathcal{G}_{43} & \mathcal{F}_4 \end{vmatrix} = \begin{vmatrix} \frac{\partial f_w}{\partial S_w} - \lambda\varphi & \frac{\partial f_w}{\partial S_g} \\ \frac{\partial f_g}{\partial S_w} & \frac{\partial f_g}{\partial S_g} - \lambda\varphi \end{vmatrix} \cdot \begin{vmatrix} A^0_{23} - \lambda A^1_{23} & A_2 \\ \mathcal{F}_{43} - \lambda\mathcal{G}_{43} & \mathcal{F}_4 \end{vmatrix}. \tag{4.10}$$

Let us define

$$\Delta H_T = \frac{\left(H_g - H_w - \frac{\rho_{gv}}{\rho_V}\left(H_o - H_w\right)\right)\left(\frac{\rho_{gw}}{\rho_W}\right)' + \left(H_g - H_o + \frac{\rho_{gw}}{\rho_W}\left(H_o - H_w\right)\right)\left(\frac{\rho_{gv}}{\rho_V}\right)'}{1 - \frac{\rho_{gv}}{\rho_V} - \frac{\rho_{gw}}{\rho_W}}.$$

where the primes indicate differentiation relative to temperature. We obtain

$$\mathcal{F}_{43} = \Delta H_T f_g + H_o' + \left(H_w' - H_o'\right) f_w + \left(H_g' - H_o'\right) f_g,$$

and

$$\mathcal{G}_{43} = \varphi \Delta H_T S_g + H_r' + \varphi\left(H_o' + \left(H_w' - H_o'\right) S_w + \left(H_g' - H_o'\right) S_g\right).$$

Furthermore

$$\mathcal{F}_4 = \frac{H_g - \frac{\rho_{gw}}{\rho_W} H_w - \frac{\rho_{gv}}{\rho_V} H_o}{1 - \frac{\rho_{gv}}{\rho_V} - \frac{\rho_{gw}}{\rho_W}}, \qquad A_2 = \frac{1 - v_{ov}}{1 - \frac{\rho_{gv}}{\rho_V} - \frac{\rho_{gw}}{\rho_W}} \frac{\rho_{gv}}{\rho_V}, \tag{4.11}$$

$$A_{23}^0 = \left(1 - v_{ov}\right) f_g \frac{\left(\frac{\rho_{gv}}{\rho_V}\right)'\left(1 - \frac{\rho_{gw}}{\rho_W}\right) + \left(\frac{\rho_{gw}}{\rho_W}\right)'\frac{\rho_{gv}}{\rho_V}}{1 - \frac{\rho_{gv}}{\rho_V} - \frac{\rho_{gw}}{\rho_W}} - v_{ov}' f_o, \tag{4.12}$$

and

$$A_{23}^1 = \left(1 - v_{ov}\right) \varphi S_g \frac{\left(\frac{\rho_{gv}}{\rho_V}\right)'\left(1 - \frac{\rho_{gw}}{\rho_W}\right) + \left(\frac{\rho_{gw}}{\rho_W}\right)'\frac{\rho_{gv}}{\rho_V}}{1 - \frac{\rho_{gv}}{\rho_V} - \frac{\rho_{gw}}{\rho_W}} + \varphi v_{ov}' S_o. \tag{4.13}$$

Let us define $tr = \frac{\partial f_w}{\partial S_w} + \frac{\partial f_g}{\partial S_g}$ and $disc = \left(\frac{\partial f_w}{\partial S_w} - \frac{\partial f_g}{\partial S_g}\right)^2 + 4\frac{\partial f_w}{\partial S_g}\frac{\partial f_g}{\partial S_w}$. The slow and fast characteristic speeds for saturation rarefaction waves are given as

$$\lambda_{S,1} = \frac{1}{2\varphi}\left(tr - \sqrt{disc}\right), \qquad \lambda_{S,2} = \frac{1}{2\varphi}\left(tr + \sqrt{disc}\right). \tag{4.14}$$

The corresponding characteristic vectors have constant T, u; only the saturations vary along these waves. Within the saturation triangle, spanned by S_w, S_o, S_g, which add to one, there is a point where $disc = 0$. Here the two characteristic speeds coincide, giving rise to a rich wave structure (see e.g. [21]).

The evaporation characteristic speed is

$$\lambda_e = \lambda_e\left(S_w, S_g, T\right) = \frac{1}{\varphi}\frac{A_2\mathcal{F}_{43} - A_{23}^0\mathcal{F}_4}{A_2\widetilde{\mathcal{G}}_{43} + A_{23}^1\mathcal{F}_4}. \tag{4.15}$$

Along evaporation rarefaction waves all quantities vary.

4.2.2. *Two-phase flow.* In the absence of the gaseous phase, there are three kinds of rarefaction waves. The thermal rarefaction wave, along which S_w, ρ_{ov}, T change. Its speed is:

$$\lambda_T = \frac{H_o' + \left(H_w' - H_o'\right) f_w}{\varphi\left(H_r' + H_o' + \left(H_w' - H_o'\right) S_w\right)}. \tag{4.16}$$

Then we have the Buckley-Leverett rarefaction with speed λ_{BL}, along which the liquid saturation S_w changes. Finally we have the composition wave with speed λ_C, which is a contact discontinuity, along which the composition and liquid water saturation change. The speeds are

$$\lambda_{BL}\left(S_w, \rho_{ov}, T\right) = \frac{1}{\varphi}\frac{\partial f_w}{\partial S_w}, \quad \lambda_C\left(S_w, \rho_{ov}, T\right) = \frac{1}{\varphi}\frac{1 - f_w}{1 - S_w}. \tag{4.17}$$

5. Numerical solution of the equations

We will use the notation $\mathcal{V} = (S_w, S_g, T)$ in the three-phase region and $\mathcal{V} = (S_w, v_{ov}, T)$ in the two-phase liquid region.

5.1. **Upstream scheme.** Consider Eqs. (3.3), where the fluxes F_ℓ are functions of $\mathcal{V}$. We can write the upstream implicit finite difference scheme ($\ell = w, v, o, T$)

$$G_\ell^m(t+\Delta t) + u^m\,(t+\Delta t)\,F_\ell^m\,(t+\Delta t) = G_\ell^m(t) + (\Delta t/\Delta x)\,u^{m-1}\,(t+\Delta t)\,F_\ell^{m-1}\,(t+\Delta t)\,, \tag{5.1}$$

where m denotes the grid cell number. The unknowns are $u^m\,(t+\Delta t)$, and the three components of $\mathcal{V}^m\,(t+\Delta t)$, which show up in the expressions for $G_\ell^m(t+\Delta t)$ and $F_\ell^m\,(t+\Delta t)$.

Let us rewrite Eq. (5.1) and shorten the unknowns as follows: $u^m\,(t+\Delta t)$ as u and $\mathcal{V}^m\,(t+\Delta t)$ as $\mathcal{V}$. We obtain the non-linear implicit scheme

$$G_\ell(\mathcal{V}) + (\Delta t/\Delta x)\,uF_\ell(\mathcal{V}) = R_\ell^{m,m-1}, \tag{5.2}$$

where we have introduced the notation $R_\ell^{m,m-1}$ for the right hand side of Eq. (5.1). We assume that $F_\ell^{m-1}(t+\Delta t)$ and $u^{m-1}(t+\Delta t)$ have been precomputed when solving the previous cell $m-1$, which may be in a phase conditions different from that of cell m. We emphasize that $R_\ell^{m,m-1}$ does not depend on the condition of cell m at the new time $t+\Delta t$.

5.2. **Solution of the non-linear system.** The system (5.2) is solved using Newton-Raphson. Given an approximate solution in the k^{th} iteration $\mathcal{V}^k$ and u^k of Eq. (5.2) we find a better approximation in the $(k+1)^{th}$ iteration. Let us define $\mathcal{R}_\ell^k$ ($\ell = w, v, d, T$) as

$$\mathcal{R}_\ell^k = G_\ell(\mathcal{V}^k) + (\Delta t/\Delta x)\,u^k F_\ell(\mathcal{V}^k) - R_\ell^{m,m-1},$$

and Eq. (5.2) becomes

$$0 = G_\ell(\mathcal{V}^{k+1}) + (\Delta t/\Delta x)\,u^{k+1} F_\ell(\mathcal{V}^{k+1}) - R_\ell^{m,m-1}.$$

Substituting $\mathcal{V}^{k+1} = \mathcal{V}^k + d\mathcal{V}$, $u^{k+1} = u^k + du$, defining $d\widetilde{u} = \Delta t/\Delta x\; du$ and neglecting second order terms we obtain

$$\left(\frac{\partial G_\ell}{\partial \mathcal{V}}(\mathcal{V}^k) + \frac{\Delta t}{\Delta x}u^k\frac{\partial F_\ell}{\partial \mathcal{V}}(\mathcal{V}^k)\right)d\mathcal{V} + \frac{\Delta t}{\Delta x}F_\ell(\mathcal{V}^k)du = -\mathcal{R}_\ell^k.$$

This is solvable for $(d\mathcal{V}, du)$ if $\frac{\Delta t}{\Delta x}u$ is not a characteristic speed, which can be achieved by taking Δt small enough. We obtain a linear system to be solved at each Newton iteration:

$$\frac{u^k\Delta t}{\Delta x}M^{(4)}(\mathcal{V}, \frac{\Delta x}{u^k\Delta t})\begin{pmatrix} d\mathcal{V}_1 \\ d\mathcal{V}_2 \\ d\mathcal{V}_3 \\ du \end{pmatrix} = \frac{u^k\Delta t}{\Delta x}\begin{pmatrix} -\mathcal{R}_1^k \\ -\mathcal{R}_2^k \\ -\mathcal{R}_3^k \\ -\mathcal{R}_4^k \end{pmatrix}. \tag{5.3}$$

5.3. **Numerical implementation.** The quantities in the grid cells are computed in the injection-production direction from the left to the right. We specify the fluxes of all components at the injection boundary. Initially all cells contain only water and oil at low temperature.

All calculations in the Newton-Raphson scheme depend on the old phase situation of cell m, as well as on available information from cells to the left of cell m. The method of solution depends on the new conditions of the cell, two-phase or three-phase.

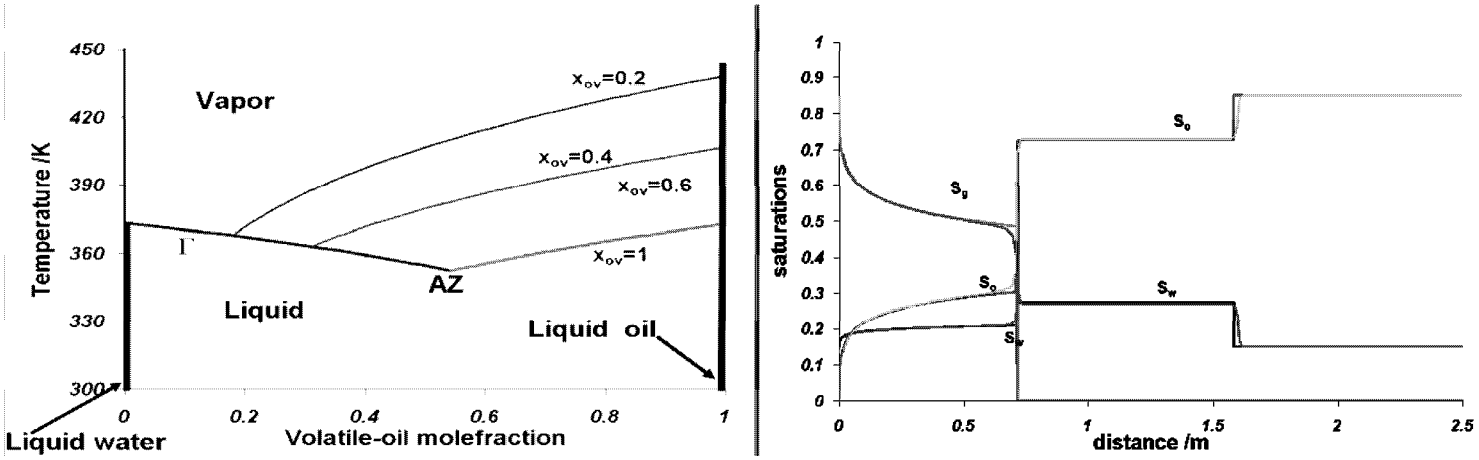

FIGURE 6.1. Left: phase diagram for water, dead oil and volatile oil (heptane) and azeotropic point. Right: comparison of MOC solution with the FD solution for the case that neither volatile oil is injected nor present in the initial oil. The straight curves are obtained with MOC, while the curved ones are obtained with FD.

The iterative procedure is simple for a cell that starts and stays in the same situation. When a cell starts in the two-phase situation, but in the two-phase calculation a temperature arises that exceeds the boiling temperature of the water-liquid oil mixture (see Fig. 6.1(left)) then the calculation is replaced by a three-phase calculation.

Simulations use a uniform grid with 2000 blocks. This implicit method is inexpensive as it only involves the solution of many 3×3 matrices as opposed to a single big matrix. As far as the authors are concerned, this finite volume method is original in the way the total velocity is treated, as there is no time derivative for it in the system.

6. Method of characteristics for steam injection

Figure 6.1(right) compares the numerical solutions obtained by the current finite difference scheme (FD) and by the Method of Characteristics (MOC) used in [11] for the saturations (S_w, S_o, S_g) versus the length along the cylinder for pure steam injection in a cylinder filled initially with dead oil only. The profiles are shown after the injection of 0.057 P(ore) V(olume) (cold water equivalent). In the steam zone where $S_g > 0$, we observe a saturation rarefaction wave and the temperature and Darcy velocity are constant. At the steam condensation front (SCF), where the temperature drops to the initial temperature, the gas saturation drops to zero. The water saturation is larger than the initial water saturation ($S_{wc} = 0.15$), both upstream and directly downstream of the SCF. Further downstream of the SCF there is a second shock to the initial conditions, i.e., $S_w = S_{wc}$, $S_o = 1 - S_{wc}$. The total downstream Darcy velocity divided by the injection velocity is constant spatially at 1.19×10^{-3} in the entire liquid zone, but it shows fluctuations of 20% between time steps. Nevertheless the average is correct. The oil saturation at the SCF is about 0.3. The observed behavior is approximately independent of the number of grid blocks. The temperature and the total Darcy velocity are not plotted because they only change at the SCF.

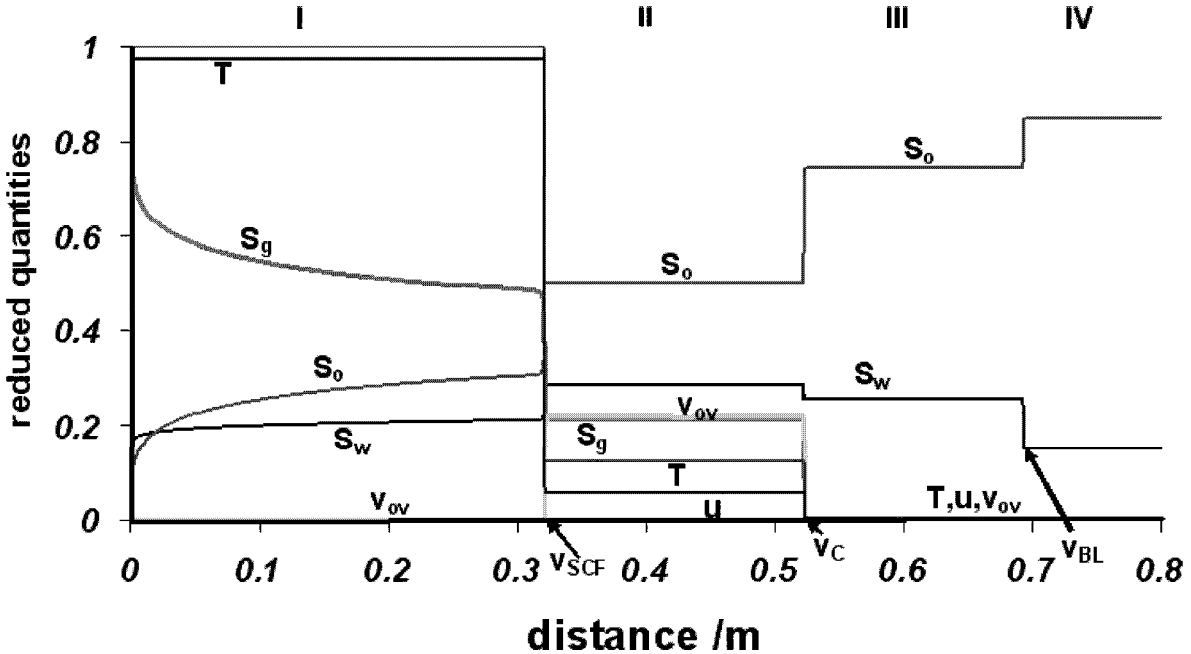

FIGURE 7.1. Steam/cyclobutane displacement of dead oil.

7. Results

The initial conditions for all the results are the following. The initial temperature is $293K$ and the gas saturation is zero. The initial water saturation is given as $S_w = S_{wc} = 0.15$. We consider the cases where the initial oil is dead oil and where the initial oil is a volumetric 50% mixture of dead oil and volatile oil; however, for cyclobutane we use a volumetric 20% mixture of dead oil and volatile oil, as 50% is above the solubility limit. In the former case we inject an alkane/steam mixture with mass fraction 0.2 (alkane/(alkane + steam)). In the latter case we displace with pure steam. The injection temperature is 373 K and injection pressure is one atmosphere. We use atmospheric pressure, because these results are most easily validated with laboratory experiments. The volumetric injection flux is 9.52×10^{-4} m/s. All figures below plot reduced quantities versus the distance. The reduced velocity (u) is the total Darcy velocity divided by the injection velocity. The reduced temperature (T) is $(T - T^{ini}) / (T_b^w - T^{ini})$. The reduced concentration (volume fraction) is $v_{ov} = \rho_{ov}/\rho_V$.

To damp transient quickly long runs were subdivided in smaller ones; in each one the initial data consisted of the previous one, where every other grid data was omitted [29]. Each run was stopped before breakthrough of the fastest wave, i.e. before it reaches the end boundary.

7.1. **Cyclobutane/steam mixture displacing dead oil.** Figure 7.1 shows displacement of dead oil by steam/cyclobutane. There are four regions from the injection point to the initial situation. In Region I, there is a fast three-phase saturation rarefaction wave with constant T and u with wave speed given by Eq. (4.14)(right); the volatile oil concentration (v_{ov}) is a small constant. The steam condensation front (SCF) separates Region I from Region II. In Region II the temperature and the total velocity are constant, but much lower

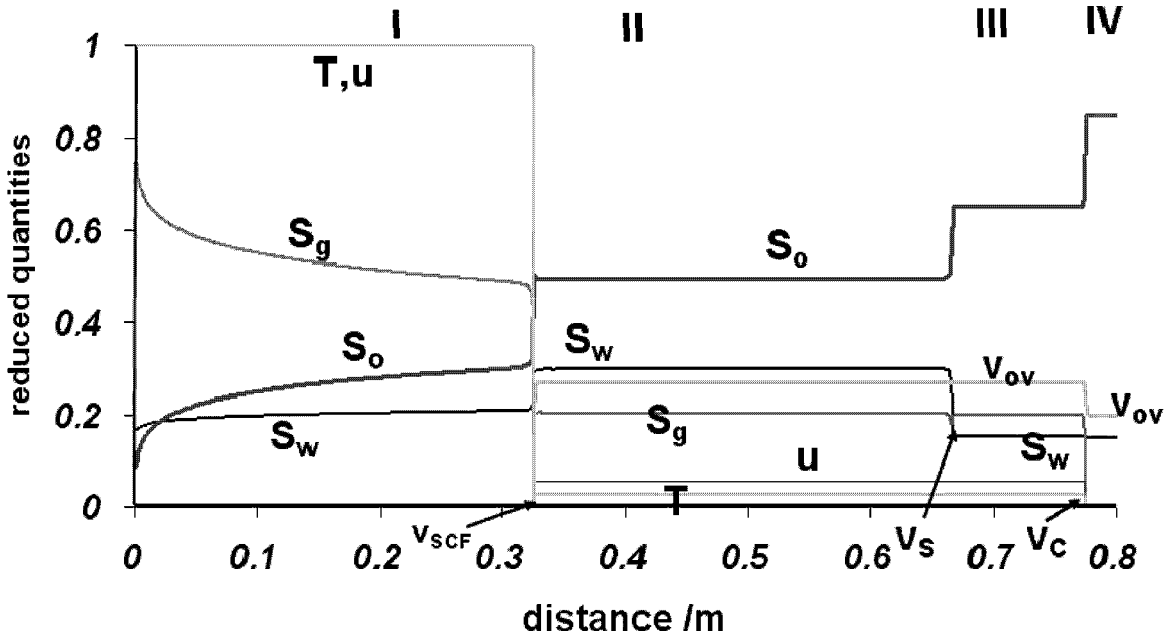

FIGURE 7.2. Steam displacement of a dead-oil/cyclobutane mixture.

than in Region I. Region I, II are three-phase regions, whereas region III and IV are two-phase liquid regions. Region II and III are separated by a cyclobutane evaporation shock, where the temperature jumps to its initial value in the reservoir and the total velocity to its final downstream value. There is a constant state in Region III. Region III and IV are separated by a Buckley-Leverett shock. Region IV contains the initial saturations.

The rarefaction in Region I starts at the injection state $(S_{wc}, 1 - S_{wc}, T_b^w, u_{inj})$ and ends at the left state of the SCF, $\left(S_{w,SCF}^-, S_{g,SCF}^-, T_b^w, u_{inj}\right)$. The right state of the SCF is $\left(S_{w,SCF}^+, S_{g,SCF}^+, T_{SCF}^+, u_{SCF}^+\right)$. Left and right states and v_{SCF} satisfy the RH conditions (4.1)-(4.4). The velocity v_{SCF} is the same as the speed of fast three-phase rarefaction (Eq. (4.14)) at the end of Region I, i.e., the SCF shock is left characteristic. Region II starts at $\left(S_{w,SCF}^+, S_{g,SCF}^+, T_{SCF}^+, u_{SCF}^+\right)$, which is the upstream (left) state of the cyclobutane condensation shock with speed v_C. The right state this shock is $\left(S_{w,E}^+, S_{g,E}^+ = 0, T_o, u_E^+\right)$. Left and right states and v_E satisfy the RH conditions (4.1)-(4.4). Region III starts with a constant state. Therefore $\left(S_{w,E}^+, S_{g,E}^+ = 0, T_o, u_E^+\right)$ is the upstream (left) state of the Buckley-Leverett shock.

7.2. **Pure steam displacing a dead-oil/cyclobutane mixture.** See Fig. 7.2. There are four regions again. In Region I, there is a fast three-phase saturation rarefaction wave at constant T and u. Separating Region I from Region II there is the SCF. Note that the temperature at the right side of the SCF is not the initial reservoir temperature, but an intermediate temperature. Region II consists of a constant state with the temperature and the total velocity lower than in Region I. Region II and III are separated by a three-phase saturation shock, which does not change the temperature but reduces the water saturation to

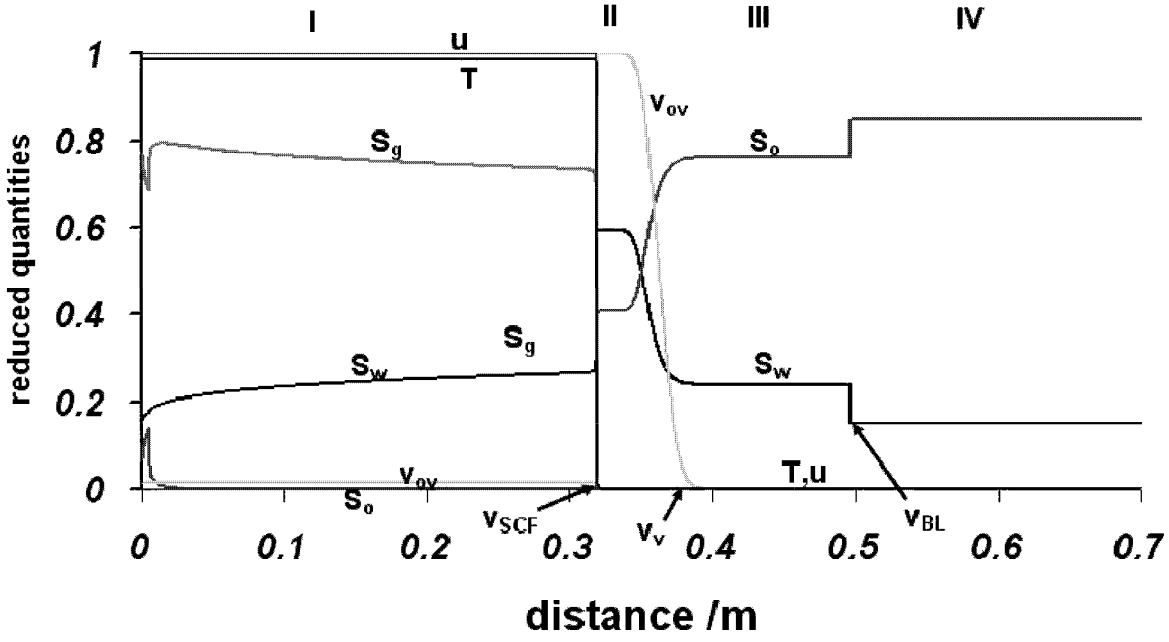

FIGURE 7.3. Steam/heptane displacement of dead-oil.

its initial value. The gas saturation in region III is slightly lower than in region II. Between region III and region IV there is a cyclobutane condensation shock.

Region I ($v_{ov} = 0$) starts at the injection state $(S_{wc}, S_g = 1 - S_{wc}, T_b^w, u_{inj})$ and ends at $\left(S^-_{w,SCF}, S^-_{g,SCF}, T_b^w, u_{inj}\right)$, which is the left state of the SCF. The right state of the SCF is $\left(S^+_{w,SCF}, S^+_{g,SCF}, T^+_{SCF}, u^+_{SCF}\right)$. Left and right states and v_{SCF} satisfy the RH conditions (4.1)-(4.4). The SCF is left characteristic. Region II consists of the constant state $\left(S^+_{w,SCF}, S^+_{g,SCF}, T^+_{SCF}, u^+_{SCF}\right)$. Region II ends at the three-phase saturation shock with speed v_S. The right state is denoted as $\left(S^+_{w,S}, S^+_{g,S}, T^+_{SCF}, u^+_{SCF}\right)$ and continues in Region III. This constant state ends at the condensation shock with speed v_C. Region IV is the right state of this shock, with initial reservoir saturation.

7.3. **Steam/heptane mixture displacing a dead-oil.** See Fig. 7.3. In Region I, there is again a fast three-phase saturation rarefaction. At the SCF the temperature drops to the initial temperature, and a volatile oil bank (Region II) builds up downstream of the SCF. The volatile oil bank does not contain any dead oil. Such pure volatile oil bank displaces all dead oil. Downstream of the volatile oil bank there is a contact wave, that marks the boundary between region II and III. The contact wave is smooth in the simulation due to numerical diffusion. Downstream there is only dead oil. Region III consists of a constant state. Region III and Region IV are separated by a Buckley-Leverett shock.

Region I starts at the injection state $(S_{wc}, S_g = 1 - S_{wc}, T^{inj}, u_{inj})$, and it ends at the left state of the SCF, viz. $\left(S^-_{w,SCF}, S^-_{g,SCF}, T^{inj}, u_{inj}\right)$. Again the SCF is left characteristic. The right state of the SCF is $\left(S^+_{w,SCF}, S^+_{g,SCF}, v_{ov} = 1, T_o, u^+\right)$ and continues as the constant state in region II. Between region II and III there is the volatile oil contact wave with right state $\left(S^+_{w,C}, S^+_{g,C}, v_{ov} = 0, T_o, u^+\right)$ and velocity v_v. Downstream of the contact wave the constant

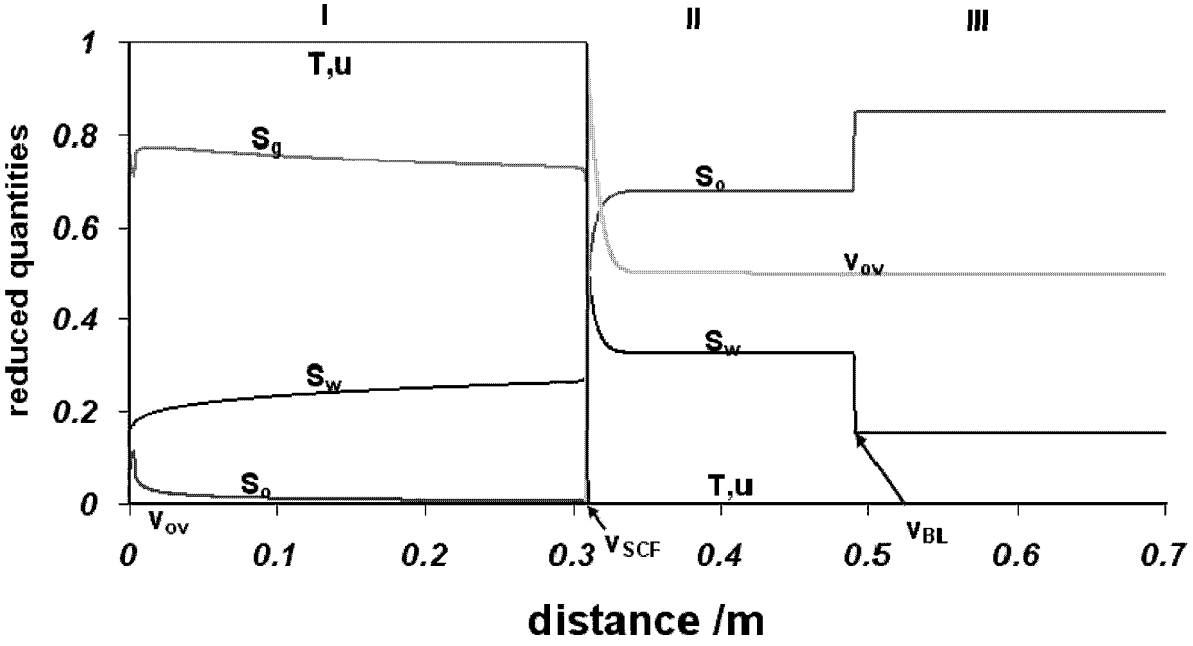

FIGURE 7.4. Steam displacement of a dead-oil/heptane mixture.

state $\left(S^+_{w,C}, S^+_{g,C}, v_{ov} = 0, T_o, u^+\right)$ spans Region III. The Buckley-Leverett shock separates Region III from Region IV. This solution agrees with the observation, made previously by JB and collaborators in the laboratory experiments [6], [10]. This is the case when analytical, numerical and experimental results are all available. They all agree.

7.4. **Pure steam displacing a dead-oil/heptane mixture.** See Fig. 7.4. There are only three regions. In Region I, there is the usual rarefaction wave with constant T and u. Separating Region I from Region II there is the SCF. In Region II the temperature is equal to the initial temperature and the total velocity attains its constant downstream value. At the SCF there is a remarkable spike of volatile oil. Left of the spike $v_{ov} = 0$. Region II consists of a constant state. Region II and III are separated by a Buckley-Leverett shock. Region III contains the initial saturations.

Region I starts at the injection state $(S_{wc}, S_g = 1 - S_{wc}, T^w_b, u_{inj})$ and ends at the left state of the SCF i.e. $\left(S^-_{w,SCF}, S^-_{g,SCF}, T^w_b, u_{inj}\right)$. The right state is $\left(S^+_{w,SCF}, S^+_{g,SCF} = 0, T_o, u^+\right)$. Left and right states and v_{SCF} satisfy the RH conditions (4.1)-(4.4). Again the SCF is left characteristic. Region II consists of the constant state $\left(S^+_{w,SCF}, S^+_{g,SCF} = 0, T_o, u^+\right)$. A Buckley-Leverett shock with velocity v_{BL} separates Region II from Region III.

Let us discuss the evolution of the volatile oil bank. Initially it does not exist. It starts to be formed after injection. It grows as long as the steam zone "swallows" the volatile oil-dead oil mixture. Growth of condensed volatile oil bank stops as soon as displacement becomes complete, because the source volatile oil ceases to be in contact with the bank.

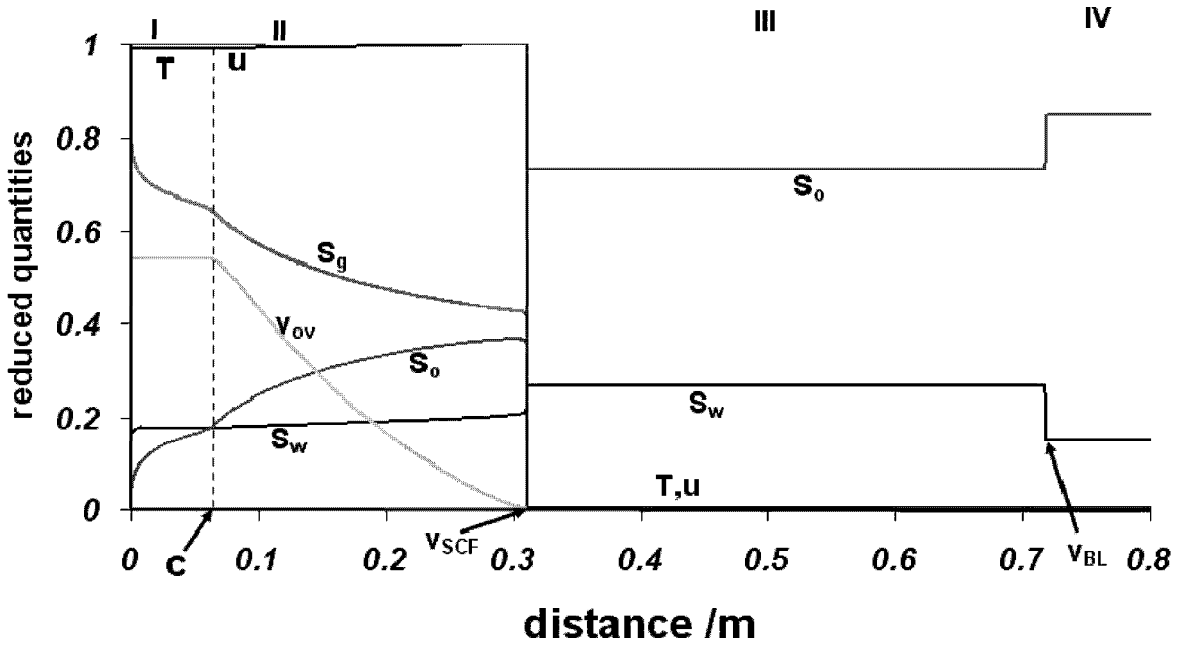

FIGURE 7.5. Steam/dodecane displacement of dead-oil. The dashed line, marked with "**c**", gives the transition from a constant temperature wave to an evaporation wave.

7.5. **Steam/dodecane mixture displacing dead-oil.** See Fig. 7.5. Besides the fast three-phase saturation rarefaction in region I, there is a volatile oil condensation wave in region II with velocity (4.15), where both T, u vary. At the state C joining rarefactions in I and II the two characteristic speeds coincide. Region II is separated from Region III by the SCF. Region III consists of a constant state, which is separated from Region IV by a Buckley-Leverett shock.

Region I starts at the injection state $(S_{wc}, S_g = 1 - S_{wc}, T^{inj}, u_{inj})$ and it ends at the coincidence point $(S_{w,C}, S_{g,C}, T^{inj}, u_{inj})$, the left state of the condensation rarefaction. The three-phase rarefaction wave is continued as a condensation rarefaction wave, which is connected to the SCF. The left state $\left(S^-_{w,SCF}, S^-_{g,SCF}, T^w_b, u^-\right)$, the right state $\left(S^+_{w,SCF}, S_g = 0, T_o, u^+\right)$ and v_{SCF} satisfy the RH conditions (4.1)-(4.4). The SCF is left characteristic.

7.6. **Pure steam displacing dead-oil/dodecane mixture.** See Fig. 7.6. There are five regions. In Region I, there is a three-phase saturation rarefaction. Near the injection point, and at some other points very small transient effects are observed. Region II consists of a constant state starting approximately at distance 0.1. Separating Region II from Region III there is a dodecane evaporation shock, followed by a fast composition rarefaction wave. The evaporation shock speed v_E coincides with the speed of the left part of the composition rarefaction wave. In Region III the temperature and the total velocity are lower than in Region I. Region III and IV are separated by the SCF, which is characteristic on the left. The temperature drops to its initial reservoir value and the total velocity to its final downstream value. There is only a constant state in Region IV. Region IV and V are separated by a Buckley-Leverett shock with speed v_{BL}. Region V contains the initial saturations.

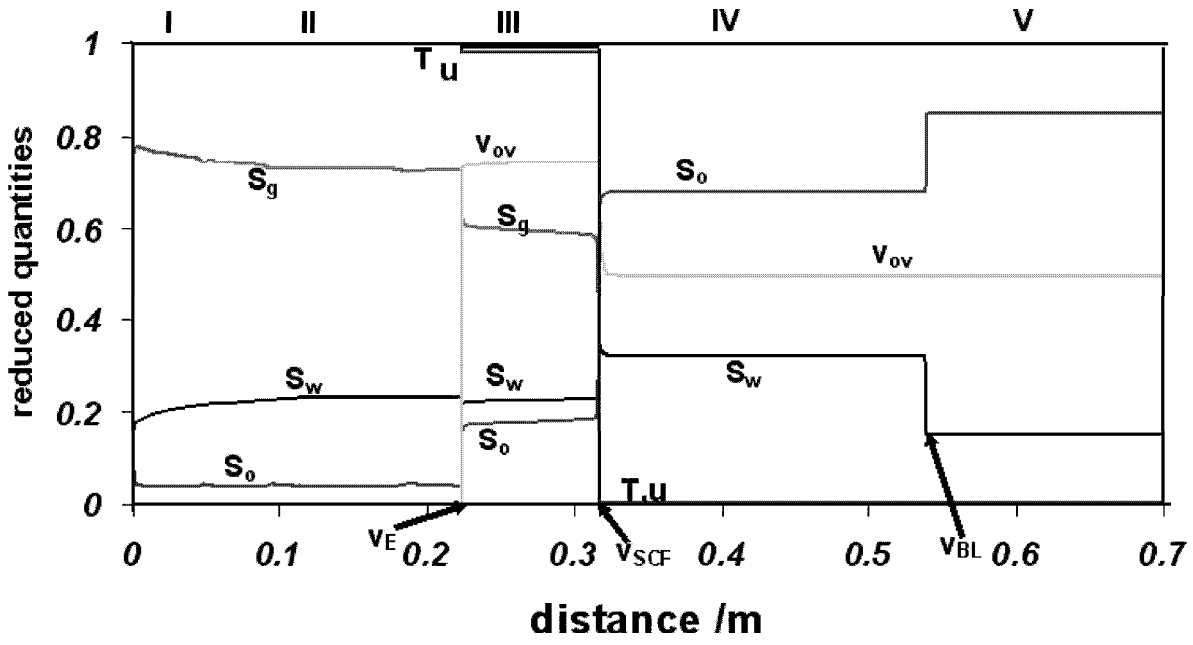

FIGURE 7.6. Steam displacement of a dead-oil/dodecane mixture

Region I starts at the injection state $(S_w, S_g, T, u) = (S_{wc}, 1 - S_{wc}, T_b^w, u_{inj})$ and ends at $\left(S_{w,E}^-, S_{g,E}^-, T_b^w, u_{inj}\right)$. Also $\left(S_{w,E}^-, S_{g,E}^-, T_b^w, u_{inj}\right)$ represents the left side of the dodecane evaporation shock as Region II is a constant state. The dodecane evaporation shock has speed v_E and right state $\left(S_{w,E}^+, S_{g,E}^+, T_E^+, u_E^+\right)$. Left and right states and v_E satisfy the RH Eqs. (4.1)-(4.4). The evaporation shock is also left characteristic. Region III starts at $\left(S_{w,E}^+, S_{g,E}^+, T_E^+, u_E^+\right)$ with a composition rarefaction, which ends at $\left(S_{w,SCF}^-, S_{g,SCF}^-, T_E^-, u_E^-\right)$, the left state of the SCF.

The right state of the SCF is $\left(S_{w,SCF}^+, S_{g,SCF}^+ = 0, T_o, u_{SCF}^+\right)$. Left and right states and v_{SCF} satisfy the RH conditions. The SCF is left characteristic. Region IV starts with a constant state and ends with a Buckley-Leverett shock.

8. CONCLUSIONS

We developed a numerical model that captures the main physical features of thermal three phase flow, involving steam, dead oil and volatile oil. The numerical solutions for different injected mixtures and initial oil composition are validated using the semi-analytic rarefaction and shock solutions. Diffusional effects are numerical.

In the 1-D setting, co-injection of medium boiling temperature volatile oil in steam leads to 100% recovery of oil. This is due to the formation of an increasingly long volatile oil bank displacing the oil in place. The presence of medium boiling temperature volatile initially also improves oil recovery. This is due to the formation of a thin volatile oil bank displacing the oil in place. Clearly the volatile oil bank displaces all the dead oil because they are in the same phase. This solution agrees with the observations found previously in the laboratory experiments. There is agreement between analytical, numerical and experimental results.

The initial presence of medium boiling temperature volatile has also a positive effect on the recovery efficiency. The initial presence of high boiling temperature volatile has only a small positive effect on the recovery efficiency. Co-injection of high boiling temperature volatile oil in steam has no effect on recovery efficiency. Co-injected or initially present low boiling temperature volatile oil has no effect on the recovery efficiency.

The essential mechanism for good recovery is that all the volatile oil condenses and remains at the point where the steam condenses.

Acknowledgments

This work follows the brilliant inspiration by Daan N. Dietz. Experimental evidence was also gathered in the MSc. theses of A. Emke, G. Metselaer, J.W. Scholten, D.W. van Batenburg, R. Quak, and C.T.S. Palmgren. This paper was initiated at the Institute for Mathematics and its Applications in Minnesota with NSF support. We thank Hans van Duijn for his early participation in this effort. We thank the anonymous referee for valuable comments and the astute observation that once the liquid volatile oil zone has been established pure steam injection can be resumed. We thank TU-Delft and IMPA for their hospitality and support. We thank B. Gundelach for her expert type setting.

References

[1] S.M. Farouq Ali and B. Abad. Bitumen recovery from oil sands, using solvent in conjunction with steam. *J. Cdn. Pet. Tech.*, pages 80–90, 1976.

[2] J. Bear. *Dynamics of Fluids in Porous Media.* Dover Publications, Inc., Dover, 1972.

[3] C. Betz, A. Farbar, and R. Schmidt. *Removing Volatile and Semi-Volatile Contaminants from the Unsaturated Zone by Injection of a Steam Air Mixture.* Thomas Telford, 1998. Contaminated Soil.

[4] R.B. Bird, W.E. Stewart, and E.N. Lightfoot. *Transport Phenomena.* John-Wiley, New York etc., 1960.

[5] R.H. Brooks and A.T. Corey. Properties of porous media affecting fluid flow. *J. Irrig. Drain. Div.*, 6:61, 1966.

[6] J. Bruining, D.N. Dietz, A. Emke, G. Metselaar, and J.W. Scholten. Improved recovery of heavy oil by steam with added distillables. *3rd European Meeting on Improved Oil Recovery, Rome*, Proc I:371–378, 1985.

[7] J. Bruining and D. Marchesin. Nitrogen and steam injection in a porous medium with water. *Transport in Porous Media (to be published)*, 2006.

[8] J. Bruining, D. Marchesin, and S. Schechter. Steam condensation waves in water-saturated porous rock. *Qualitative Theory of Dynamical Systems*, 5:81–106, 2004.

[9] J. Bruining, D. Marchesin, and C.J. van Duijn. Steam injection into water-saturated porous rock. *Comp. Appl. Math.*, 22 (3):359–395, 2004. Informes de Matemtica (IMPA-Preprints), www.preprint.impa.br A-136 2002.

[10] J. Bruining, D.W. van Batenburg, H.J. de Haan, R. Quak, and C.T.S. Palmgren. The efficiency of the distillation mechanisms to enhance steamdrive recovery. *Proc. of the 4th Symposium on Enhanced Oil Recovery, Hamburg*, October:887–898, 1987.

[11] J. Bruining and C.J. van Duijn. Uniqueness conditions in a hyperbolic model for oil recovery by steam-drive. *Computational Geosciences*, 4:65–98, 2000.

[12] K.H. Coats. A highly implicit steamflood model. *Soc. of Pet. Eng. J.*, pages 369–383, 1978. SPE 6105.

[13] C.M. Dafermos. *Hyperbolic Conservation Laws in Continuum Physics.* Springer-Verlag, Berlin, 2000.

[14] R.E. Dumor'e, J. Hagoort, and A.S. Risseeuw. An analytical model for one-dimensional, three-component condensing and vaporizing gas drives. *Soc. Pet. Eng. J.*, April:169–179, 1984.

[15] A.H. Falls and W.M. Schulte. Theory of three-component, three-phase displacement in porous media. *SPE Reservoir Engineering*, pages 377–384, 1992.

[16] F. J. Fayers and J.D. Matthews. Evaluation of normalized stone's methods for estimating three-phase relative permeabilities. *Soc. Pet. Eng. J.*, pages 224–232, 1984.

[17] R.E. Guzman and F.J. Fayers. Solutions to the three-phase buckley-leverett problem. *SPE Journal*, 2:301–311, 1997.
[18] E.J. Hanzlik and D.S. Mims. Forty years of steam injection in california-evolution of heat management. *SPE International Improved Oil Recovery Conference in Asia Kuala Lumpur Malaysia*, SPE 84848, 2003.
[19] F.G. Hirasaki. Application of the theory of multicomponent multiphase displacement to thee component, two-phase surfactant flooding. *Soc. Pet. Eng. J.*, April:191–204, 1981.
[20] E. Isaacson, D. Marchesin, and B. Plohr. Transitional waves for conservation laws. *SIAM J. Math. Anal.*, 21:837–866, 1990.
[21] E. Isaacson, D. Marchesin, B. Plohr, and J.B. Temple. Multi-phase flow models with singular riemann problems. *Mat. Apl. Comput.*, 2:147–166, 1992.
[22] R. Juanes and T.W. Patzek. Analytical solution to the riemann problem of three-phase flow in porous media. *Transport in Porous Media*, 55:47–70, 2004.
[23] S.F. Kaslusky and K.S. Udell. A theoretical model of air and steam co-injection to prevent the downward migration of the dnapl's during steam enhanced extraction. *Journal of Contaminant Hydrology*, 55:213–232, 2002.
[24] L.W. Lake. *Enhanced Oil Recovery*. Prentice Hall International, Englewood Cliffs, 1989.
[25] G. Mandl and C.W. Volek. Heat and mass transport in steamdrive processes. *Soc. Pet. Eng. J.*, pages 57–79, 1969.
[26] D. Marchesin and B.J. Plohr. Wave structure in wag recovery, spe 71314. *SPEJ*, 6 (2):209–219, 2001.
[27] W.J. Moore. *Physical Chemistry*. Prentice Hall, 1962.
[28] V. Oballa, D.A. Coombe, and W.L. Buchanan. Adaptive-implicit method in thermal simulation. *SPE Reservoir Engineering*, pages 549–556, 1990.
[29] B.J. Plohr. Private communication. 2000.
[30] G.A. Pope. The application of fractional flow theory to enhanced oil recovery. *Soc. Pet. Eng. J.*, 20:191–205, 1980.
[31] W.R. Shu and K.J. Hartman. Effect of solvent on steam recovery of heavy oil. *SPE Reservoir Engineering*, SPE 14223:457–465, 1988.
[32] N.D. Shutler. A one dimensional analytical technique for predicting oil recovery by steam flooding. *Soc. Pet. Eng. J.*, pages 489–498, 1972.
[33] J. Smoller. *Shock Waves and Reaction-Diffusion Equations*. Springer-Verlag, New York, 1980.
[34] W.S. Tortike and S.M. Farouq-Ali. Saturated-steam-property functional correlations for fully implicit thermal reservoir simulation. *SPE Reservoir Engineering*, 4 (4):471–474, 1989.
[35] K.S. Udell and L.D. Stewart. Combined steam lnjection and vacuum extraction for aquifer cleanup. keynote paper. *Conference of the International Association of Hydrogeologists*, Calgary, Canada, 1990.
[36] R.C. Weast. *CRC Handbook of Chemistry and Physics* 58^{th} *edition*. CRC Press, Inc., New York, 1977-1978.
[37] B.T. Willman, V.V. Valeroy, G.W. Runberg, and A.J. Cornelius. Laboratory studies of oil recovery by steam injection. *Journal of Petroleum Technology*, pages 681–690, 1961.
[38] J.S. Wingard and F.M. Orr. An analytical solution for steam/oil/water displacements. *SPE Advanced Technology Series*, 2:167–176, 1994.
[39] C.L. Yaws. *Chemical Properties Handbook*. McGraw-Hill, New York, 1999.
[40] Y.C. Yortsos. Distribution of fluid phases within the steam zone in steam injection processes. *Soc. Pet. Eng. J.*, pages 458–466, 1984.

Appendix A. Physical quantities; symbols and values

In this Appendix we summarize the values and units of the various quantities used in the computation and empirical expressions for the various parameter functions. All enthalpies per unit mass are with respect to the enthalpies at the reference temperature of the components in their standard form. All heat capacities are at constant pressure. All enthalpies in their standard form are zero at the reference temperature.

A.1. **Temperature dependent properties of steam and water.** We use references [34], [39] and [36] to obtain all the temperature dependent properties below.

The rock enthalpy is expressed as

$$H_r = (1-\varphi)\, c_{prock}\left(T-\bar{T}\right), \quad c_{prock} = 3.274 \times 10^6 J/m^3/K. \tag{A.1}$$

The liquid water enthalpy $h_W(T)$ [J/kg] as a function of temperature is approximated by

$$h_W(T) = 4184.0\left(T-\bar{T}\right). \tag{A.2}$$

A conventional choice for the reference temperature is $\bar{T} = 298.15K$. The heptane enthalpy $h_{oV}[J/kg]$ and the dead oil enthalpy h_{oD} as a function of temperature is approximated by

$$h_{oV}(T) = c_{oV}\left(T-\bar{T}\right), \qquad h_{oD}(T) = c_{oD}\left(T-\bar{T}\right). \tag{A.3}$$

where the values for the heat capacities for heptane and dead oil are

$$c_{oV} = 2242, \qquad c_{oD} = 1914.1 \ [J/kg/K]. \tag{A.4}$$

These enthalpies are chosen such that the enthalpy of oil per unit volume is independent of composition. Therefore the heat capacity of the oleic phase per unit volume can also be defined independently of composition. The steam enthalpy h_{gW} as a function of temperature is given by

$$h_{gW}(T) = h^s_{gW}(T) + \Lambda_W(\bar{T}) \tag{A.5}$$

and the sensible steam enthalpy is approximated as

$$h^s_{gW}(T) = c_{pgw}\left(T-\bar{T}\right) \quad \text{with} \quad c_{pgw} = 1964.0. \tag{A.6}$$

The volatile oil vapor enthalpy h_{gV} as a function of temperature is given by

$$h_{gV}(T) = h^s_{gV}(T) + \Lambda_V(\bar{T}) \tag{A.7}$$

and the sensible heptane enthalpy is approximated as as

$$h^s_{gV}(T) = c_{pgv}\left(T-\bar{T}\right) \qquad \text{with} \qquad c_{pgv} = 1658.0. \tag{A.8}$$

Table: Summary of physical input parameters and variables

Physical quantity	*Symbol*	*Value*	*Unit*
Water, gas, oil fractional flows	f_w, f_g, f_o	Eq. (A.16).	[m^3/m^3]
Steam, vol-oil enthalpy/unit mass	h_{gW}, h_{gV}	Eqs. (A.5), (A.7).	[J/kg]
Sensible enthalpy/unit mass	h^s_{gW}, h^s_{gV}	Eqs. (A.6), (A.8).	[J/kg]
vol-oil, oil enthalpy/unit mass	h_{oV}, h_{oD}	Eqs. (A.3).	[J/kg]
Gas enthalpy, Oil Enthaply	H_g, H_o	$H_{gw}+H_{gv}, H_{ov}+H_{od}$	[J/m^3]
Steam, vol-oil enthalpy	H_{gW}, H_{gV}	$\rho_{gW}(T)h_{gW}(T), \rho_{gV}(T)h_{gV}(T)$	[J/m^3]
Sensible steam, vol-oil enthalpy	H^s_{gW}, H^s_{gV}	$\rho_{gW}(T)h^s_{gW}(T), \rho_{gV}(T)h^s_{gV}(T)$	[J/m^3]
Partial Steam, vol-oil enthalpy	H_{gw}, H_{gv}	$\rho_{gw}(T)h_{gW}(T), \rho_{gv}(T)h_{gV}(T)$	[J/m^3]
vol-oil, oil enthalpy	H_{oV}, H_{oD}	$\rho_V(T)h_{oV}(T), \rho_{oD}(T)h_{oD}(T)$	[J/m^3]
Partial vol-oil, oil enthalpy	H_{ov}, H_{od}	$\rho_{ov}(T)h_{oV}(T), \rho_{od}(T)h_{oD}(T)$	[J/m^3]
Rock enthalpy	H_r	$C_r(T-\bar{T})$, Eq. (A.1).	[J/m^3]
Water enthalpy	H_W	$\rho_W(T)h_W(T)$	[J/m^3]
Porous rock permeability	k	1.0×10^{-12}	[m^2]
Water, gas, oil rel. perms.	k_{rw}, k_{rg}, k_{ro}	Eq. (A.14 and A.15) .	[m^3/m^3]
Molar weight, H_2O, C_7H_{16}, d-oil	M_W, M_V, M_D	0.018, 0.10021, 0.4	[kg/mole]
Total. pressure	P	1.0135×10^5	[Pa]
Atmospheric pressure	P_o	1.0135×10^5	[Pa]
Partial pressures	P_w, P_v	Eqs. (2.3), (2.4).	[Pa]
Water, vapor, oil saturations	S_w, S_g, S_o	Independent variables.	[m^3/m^3]
Residual oil, connate water satur.	S_{or}, S_{wc}	0, 0.15	[m^3/m^3]
Injection saturations	S_w^{inj}, S_o^{inj}	input	[m^3/m^3]
Temperature	T	Independent variable.	[K]
Azeotropic temperature	$T_{az}\,(x_{ov}=1)$	Eq. (2.5).	[K]
Reservoir, injection temperature	T^{ini}, T^{inj}	293, 293 − 373.	[K]
Boiling point of water, vol. oil	T_b^w, T_b^v	373.15, 371.57 for heptane.	[K]
Total Darcy velocity	u	Volume flux of all phases.	[m^3/(m^{2}s)]
Total injection velocity	u^{inj}	Injected volume flux.	[m^3/(m^{2}s)]
Water, vol-oil evaporation heat	Λ_W, Λ_V	see Eqs. (A.9).	[J/kg]
Water, steam, oil viscosity	μ_w, μ_g, μ_o	Eqs. (A.10)-(A.13).	[Pa s]
Water, steam, vol-oil vapor density	ρ_W, ρ_{gW}, ρ_{gV}	998.2, Eqs. (2.2).	[kg/m^3]
Pure heptane, dead oil densities	ρ_V, ρ_D	683, 800	[kg/m^3]
Steam, vol-oil vapor concentrations	ρ_{gw}, ρ_{gv}	$\rho_{gW}P_w/P$, $\rho_{gV}P_v/P$, Eq. (2.2)	[kg/m^3]
Liq. vol-oil concentrations	ρ_{ov}, ρ_{od}	Obtained from Eqs. (2.6, 2.1)	[kg/m^3]
Molar fraction vol-oil in dead oil	x_{ov}	Eq. (2.5).	[-]
Rock porosity	φ	0.38	[m^3/m^3]

All of this leads to an oleic phase heat capacity per unit volume of

$$C_o = 1.531\times10^6\left[J/m^3/K\right].$$

For the latent heat $\Lambda_W(T)$ $(,\Lambda_V(T))\,[J/kg]$ or evaporation heat of water (heptane) we use

$$\Lambda_W(T) = 3.105\,6\times10^6 - 2220.0T, \qquad \Lambda_V(T) = 5.388\,3\times10^5 - 584.0T. \tag{A.9}$$

The temperature dependent liquid water viscosity $\mu_w\ [Pas]$ is approximated by

$$\mu_w = \exp\left(-12.06 + 1509/T\right). \tag{A.10}$$

The viscosity of the dead oil μ_{od} and heptane μ_{ov} is written as

$$\mu_{od} = \exp\left(-13.79 + 3781/T\right), \quad \mu_{ov} = \exp\left(-10.813 + 880.2/T\right). \tag{A.11}$$

and the viscosity of the oil mixture is approximated with the quarter power rule

$$\mu_o = \left(\frac{\rho_{ov}}{\rho_V}\mu_{ov}^{\frac{1}{4}} + \frac{\rho_{od}}{\rho_D}\mu_{od}^{\frac{1}{4}}\right)^4. \tag{A.12}$$

We assume that that the viscosity of the gas is independent of composition

$$\mu_g = 1.826\,4 \times 10^{-5}\,(T/300)^{0.6}. \tag{A.13}$$

The water saturation pressure as a function of temperature is given by Eq. 2.3. The pure phase densities of steam and volatile oil vapor are given by Eqs. (2.2) and the corresponding concentrations ρ_{gw}, ρ_{gv} are given in the Table.

A.2. **Three phase relative permeabilities.** We used Stone's expressions [16] for three-phase permeability: equations (A.14)-(A.15) describe the water relative permeability k_{rw}, the air relative permeability k_{rg} and the oil relative permeability k_{ro} respectively. For convenience we have taken the residual oil parameter used by Fayers [16] S_{om} equal to zero. The relative permeabilities k_{rw}, k_{rg} are functions of the water saturation S_w and the gas saturation S_g respectively.

$$k_{rw} = k_{rw}^{'} S_{we}^{3+2/\lambda}, \qquad k_{rg} = k_{rg}^{'}(1 - S_{ge})^2(1 - S_{ge}^{1+2/\lambda}), \tag{A.14}$$

$$k_{ro} = \frac{S_o(1 - S_{wc})}{k_{rcow}(1 - S_w)(1 - S_{wc} - S_g)} k_{row} k_{rog}, \tag{A.15}$$

$$S_{we} = \frac{S_w - S_{wc}}{1 - S_{wc} - S_{or}}, \quad S_{ge} = \frac{1 - S_g - S_{wc}}{1 - S_{wc} - S_{or}},$$

$$k_{row} = k_{rg}^{'}(1 - S_{we})^2(1 - S_{we}^{1+2/\lambda}), \quad k_{rog} = k_{rw}^{'} S_{ge}^{3+2/\lambda}.$$

We took $k_{rw}^{'} = 1/2$, $k_{rg}^{'} = 1$ and $k_{rcow} = 1$. Here $\lambda = 0.5$ is the sorting factor, S_{wc} is given in Table A.1 and $S_{or} = 0$ are the connate water saturation and the residual oil saturation respectively.

We can express the Buckley-Leverett fractional flow functions for $\alpha = o, w, g$ as

$$f_\alpha = (k_{r\alpha}/\mu_\alpha) \,/\, (k_{rw}/\mu_w + k_{ro}/\mu_o + k_{rg}/\mu_g). \tag{A.16}$$

where f_α is the fraction of the volume flux of phase α [2].

Dietz Laboratory, Centre of Technical Geoscience, Mijnbouwstraat 120, 2628 RX Delft, The Netherlands

E-mail address: J.Bruining@citg.tudelft.nl

Instituto Nacional de Matemática Pura e Aplicada, Estrada Dona Castorina 110, 22460-320 Rio de Janeiro, RJ, Brazil

E-mail address: marchesi@impa.br